J. Am. Soc. Mass Spectrom. (2019) 30:309–320
DOI: 10.1007/s13361-018-2086-8

RESEARCH ARTICLE

Quantifying SIMS of Organic Mixtures and Depth Profiles—Characterizing Matrix Effects of Fragment Ions

M. P. Seah, R. Havelund, S. J. Spencer, I. S. Gilmore

Analytical Science Division, National Physical Laboratory, Teddington, Middlesex TW11 0LW, UK

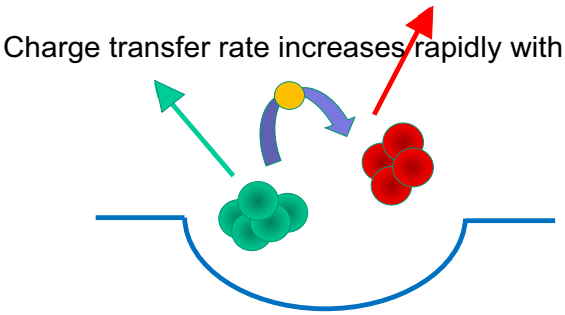

Abstract. Sets of matrix factors, Ξ, are reported for the first time for secondary ions in secondary ion mass spectrometry for several binary organic systems. These show the interplay of the effects of ion velocity, fragment chemistry, and the secondary ion point of origin. Matrix factors are reported for negative ions for Irganox 1010 with FMOC or Irganox 1098 and, for both positive and negative ions, with Ir(ppy)2(acac). For Irganox 1010/FMOC, the Ξ values for Irganox 1010 fall with m/z, whereas those for FMOC rise. For $m/z < 250$, Ξ scales very approximately with $(m/z)^{0.5}$, supporting a dependence on the ion velocity at low mass. Low-mass ions generally have low matrix factors but |Ξ| may still exceed 0.5 for $m/z < 50$. Analysis of ion sequences with addition or loss of a hydrogen atom shows that the Ξ values for Irganox 1010 and FMOC ions change by − 0.026 and 0.24 per hydrogen atom, respectively, arising from the changing charge transfer rate constant. This effect adds to that of velocity and may be associated with the nine times more hydrogen atoms in the Irganox 1010 molecule than in FMOC. For Irganox 1098/Irganox 1010, the molecular similarity leads to small |Ξ|, except for the pseudo molecular ions where the behavior follows Irganox 1010/FMOC. For Ir(ppy)2(acac)/Irganox 1010, the positive secondary ions show twice the matrix effects of negative ions. These data provide the first overall assessment of matrix factors in organic mixtures necessary for improved understanding for quantification and the precise localization of species.

Keywords: Analysis, Matrix factors, Organic solid mixtures, Quantification, Secondary ion mass spectrometry, SIMS

Received: 27 July 2018/Revised: 4 October 2018/Accepted: 5 October 2018/Published Online: 23 October 2018

Introduction

Secondary ion mass spectrometry (SIMS) has been a powerful and popular analytical method for over 50 years. It has found massive application in the semiconductor industry for the quantitative analysis of dilute quantities and for the depth profiling of dopant delta layers. For the dilute compositions involved there, the signal intensity can be linearly related to the quantity present and that signal can be calibrated using a reference sample. It was recognized that the analysis of non-dilute quantities would be difficult because of the strong matrix effects. The use of O_2^+ or Cs^- primary ion beams takes advantage of the strong matrix effect by continuously implanting these elements into the surface layer. This generates ternary systems where the proportion of the most influential element is more nearly constant. This significantly reduces the signal non-linearity with composition and also significantly increases the secondary ion signal level. Beyond recognizing that there was a matrix effect, there were no detailed quantitative studies in binary systems with unreactive beams since other techniques such as Auger electron spectroscopy (AES) or X-ray photoelectron spectroscopy (XPS) could provide the desired information at the higher compositions. However, that approach is insufficient for the modern study of organic systems where SIMS is necessary to give discrimination between similar materials that are not distinct in XPS.

The depth profiling of organic materials is conducted, today, using cluster sputtering ions that are mainly argon clusters to

Electronic supplementary material The online version of this article (https://doi.org/10.1007/s13361-018-2086-8) contains supplementary material, which is available to authorized users.

Correspondence to: M. Seah; *e-mail:* martin.seah@npl.co.uk

avoid significant damage to the underlying material. In the SIMS analysis of organic materials, there can be strong matrix effects. In the spectra, both the amounts of suppression and enhancement that occur vary in extent as the composition changes [1–3]. In 2009, Shard et al. [4] studied the matrix effect in the secondary ion emission from intimate molecular mixtures of codeine and poly(lactide) sputtered by 10 keV C_{60}^+ cluster ions and analyzed using 25 keV Bi_3^+ ions. The positive secondary ion data were interpreted in terms of a simple model of charge transfer involving proton exchange from an initially emitted positively charged secondary ion, causing it to be suppressed, to a neutral fragment whose ion signal is then enhanced. Proton transfer to provide ionized species of organic materials is a well-known process used in soft ionization methods such as matrix-assisted laser desorption ionization (MALDI) where proton donors are used as the enhancing matrices. This effect is also demonstrated in SIMS [1–3]. Shard et al. [4] give equations for the ion intensities involving two matrix parameters α and β and the composition. The difficult part of such studies is to fabricate a number of known homogeneous intimate mixtures of the two organic molecules in order to evaluate these parameters.

The overall matrix effect was summarized in 2015 [5] in a single useful parameter, Ξ, which describes the total intensity across the phase diagram compared with the result for zero enhancement. For suppression, Ξ is negative but cannot, of course, be less than -1. In the 2015 work, the materials studied were intimate mixtures of pentaerythritol tetrakis(3-(3,5-di-tert-butyl-4-hydroxyphenyl)propionate (Irganox 1010) with either N,N'-hexane-1,6-diylbis(3-(3,5-di-tert-butyl-4-hydroxyphenylpropionamide) (Irganox 1098) or fluorenylmethyloxycarbonyl-L-pentafluorophenylalanine (FMOC). The negative ions studied included the intense pseudo molecular ions and, for Irganox 1010 with Irganox 1098, exhibited Ξ values in the range -0.3 to 0.3, i.e., all had weak suppression or enhancements. For Irganox 1010 with FMOC, the Ξ values spanned the wider range -0.7 to 1.1. Although the original model was for proton exchange for positive ions [5], there is nothing, in principle, to forbid the same form of analysis applying to electron exchange [6].

We have, elsewhere [7], analyzed details of delta layers of FMOC in Irganox 1010 and found that data may be accurately described by Shard et al.'s equations [4, 5]. If the matrix effects are measured and accounted for, a consistent quantity (amount of substance) of delta-layer material may be deduced for all the negative secondary ions, despite the fact that the intensities, when normalized to those of the bulk material, ranged over a factor of more than 20, i.e., the use of a single secondary ion with an unknown matrix factor could involve errors in quantification of this magnitude. Analysis of interface positions similarly [8] shows apparent shifts of more than 20 nm for the ion signals. These intensity changes and shifts arise from matrix effects and when these are removed, a consistent interface profile is obtained for all emitted ions.

Just as in the studies of inorganic systems, matrix effects have also been used to obtain enhanced signal intensities for organic studies. These studies give some further insight. Delcorte [9] considers three changes to the sample that would enhance the signal level, (i) blending the sample with a low molecular weight organic matrix to increase the sputtering yield and enhance both ion polarities, (ii) adding a suitable salt where weak bases, e.g., aromatic molecules, are better cationized by weak acids (group Ib metal cations) and hard bases, e.g., peptides, are more efficiently ionized by hard acids (alkali cations), and (iii) depositing a noble metal such as Ag or Au on the surface leading to high levels of cationized signals.

Jones et al. [1], in their study of 1:1 organic mixtures, find that the $[M+H]^+$ ion of atropine may be almost completely suppressed by the presence of a compound (dipalmitoylphosphatidylcholine (DPPC)) of higher proton affinity. However, the intensity of the $[M-H]^-$ ion was not so affected. Jones et al. [10] show that the propensity of a molecule to form either a protonated or deprotonated ion depends upon the relative acid/base properties of the compounds present. The molecule with the higher proton affinity has a raised $[M+H]^+/[M-H]^-$ intensity ratio and that with the lower proton affinity a reduced $[M+H]^+/[M-H]^-$ intensity ratio. Karras and Lockyer [2] using similar arguments explain the strong suppression of ibuprofen intensities in a mixture with paracetamol.

The simplest analog of the $O_2^{\pm}$ sputtering beam used for inorganics is the use of water cluster ions for organic materials. Early studies used water vapor injection and Mouhib et al. [11] find an order of magnitude increase in $[M+H]^+$ signal from Irgafos 168 as the chamber pressure reached ~ 3×10^{-6} Torr, when the surface may have around a monolayer of water adsorbed. Instead of adsorbing water, later studies involved the more efficient use of primary ion water clusters. Sheraz et al. [12], studying pure drug samples, find the ion yield of "molecular" positive secondary ions, $[M+H]^+$, to be enhanced by about a factor of 10 for arginine and angiotensin II but nearer 20 for haloperidol and DPPC. The increased density of hydrogen and protons was thought critical here. In more recent work, Sheraz et al. [13] show that the sputtering yields using pure water and argon clusters are similar and that it is the ionization that is enhanced. Furthermore, with water, the molecular ion yields instead of falling as E/n is reduced below ten, as for argon clusters, rises until E/n reaches three and only fall at lower E/n values. This may parallel the effects in the $O_2^{\pm}$ sputtering used for inorganic materials where, at low energies, the reduced sputtering yield means that the important oxidation of the surface layer can reach its maximum. Sheraz et al. show, by using D_2O clusters in the beam, that the increase in ion yields arises from protonation of the molecule mainly from the bombarding water molecules.

Instead of using water cluster primary ion beams, others have tried adding acid vapor. Angerer et al. [14] expose rodent brain sections to trifluoracetic acid vapor. This, on subsequent SIMS analysis using 8% CO_2 in an argon cluster beam showed greatly enhanced lipid signals and reduced cholesterol in the

positive ion spectrum. Tian et al. [15] add 5% HCl into an argon cluster beam and condense 10 nm of D_2O on the surface of frozen-hydrated mouse brain sections. These show ~ tenfold increase in the protonated lipid species.

Thus, significant enhancements are available when using active ion beams but we do not yet have a clear understanding of the behavior for profiles made with the more basic argon gas cluster ion beam (GCIB). We need a clearer view of the behavior and mechanisms to make any quantitative measurements of either amount of substance or interface locations. This requires the manufacture of special samples with known compositions. This is difficult and so relevant work is scant. In the present work, therefore, we seek to characterize the matrix effects in three binary organic mixtures sputtered by argon clusters and analyzed using 25 keV Bi_3^+, to understand, better, the matrix behaviors in general SIMS studies of organic mixtures.

Experimental

The experimental details are described by Shard et al. [16] and are detailed further in Havelund et al. [17]. Briefly, two of the samples were made to study, inter alia, the sputtering of uniform mixtures to establish matrix effects. They contained both pure layers and three layers of uniform mixtures at volume fractions of 0.2, 0.5, and 0.8. The first sample was of FMOC ($C_{24}H_{16}F_5NO_4$, $M = 477.1$) and Irganox 1010 ($C_{73}H_{108}O_{12}$, $M = 1177.8$). The second was of Irganox 1098 ($C_{40}H_{64}N_2O_4$, $M = 636.5$) with Irganox 1010. A third sample of Bis[2-(2-pyridinyl-N)phenyl-C](2,4-pentanedionato-O2,O4)iridium(III) ($Ir(ppy)_2(acac)$ $C_{27}H_{23}IrN_2O_2$ $M = 600.1$) with Irganox 1010 contained pure layers and one of a mixture of 58.5% by volume $Ir(ppy)_2(acac)$ determined by X-ray photoelectron spectroscopy (XPS). The materials, from Sigma-Aldrich, were each sublimed in a QBox 450 (Mantis Deposition Ltd., Thame, UK) with relevant monitoring, shuttering, and sample rotation to create the 100-nm thick layers ordered as shown in Figure 1 of Shard et al. [16]. The evaporators were controlled by quartz crystal oscillators (QCOs) calibrated to relate their outputs to the thicknesses of each material deposited on the wafer substrates by ellipsometry using an M2000DI spectroscopic ellipsometer (Woollam, NE, USA). A measurement fault occurred during deposition of the Ir(ppy)2(acac)/Irganox 1010 layer requiring its composition to be measured, subsequently, by XPS.

The above multilayer samples were depth profiled by SIMS using a 5 keV Ar_{2300}^+ GCIB in an ION-TOF SIMS IV instrument (ION-TOF GmbH) with the incident ions at 45° to the surface normal. Secondary ion intensities were measured using 25 keV Bi_3^+ ions also at 45° incidence angle, but in an azimuth at 90° to the argon gas cluster sputtering beam. The sputtering beam was rastered, in interlaced mode, over an area of 500 µm by 500 µm, and the analysis was in a central zone of 200 µm by 200 µm. The relative Bi_3^+ dose was < 0.2% of the GCIB dose. Electron flood charge compensation with a 20 eV electron beam at 5 µA was used and the spectra were dead time corrected.

The XPS measurements were made in a Kratos Axis Ultra using the Al Kα monochromated X-ray beam and sputtering with 5 keV Ar_{1000}^+ ions. Quantification was made using XPS average matrix sensitivity factors [18–20] with analyzer transmission function correction [21, 22] and was confirmed using the pure material layers.

Theory

The measured intensity allowing for the enhancement for a secondary ion from A arising from a content of B, ϕ_B, has given by Shard et al. [5]. As before [23], we modify their equation to give

$$\frac{I_A/y}{I_A^\infty/y_A} = \phi_A + \phi_B\alpha_A[1-\exp(-\beta_A\phi_A)] \quad (1)$$

where I_A is the characteristic ion intensity from A in the mixture and I_A^∞ is its intensity from pure A. The parameters α_A and β_A are the enhancement parameters, y is the yield volume for the mixture, and y_A that for pure A. Since the signals are generated by 25 keV Bi_3^+ ions, the y yield volumes are for that primary ion and are limited to the yield volumes from which these ions are generated [17]. It is assumed that I_A is zero in material B and the volume fractions ϕ_A and ϕ_B sum to unity. Equation (1) differs from that by Shard et al. [5] by the inclusion of the sputtering yields for the analytical ion. The intensity for suppressed signals, assumed to be for B since it is the charge from B ions that generate A ions, is

$$\frac{I_B/y}{I_B^\infty/y_B} = \phi_B\{1 + \alpha_B[1-\exp(-\beta_A\phi_A)]\} \quad (2)$$

Equation (2), here, differs from the equivalent equation by Shard et al. [5] by changing the sign of α so that α is positive for enhancement and negative for suppression. In the original derivation [5], there were only two ions, one for each material with a number of B ions donating their charge to A neutrals to form A ions. So, as originally formulated, the gain to A came from the loss to B and hence β_A and β_B were the same and

$$\alpha_A I_A^\infty/y_A = -\alpha_B I_B^\infty/y_B \quad (3)$$

There, $-\alpha_B$ has a maximum value of unity where all of the emitted secondary ion fragments of a particular mass are available to donate their charge. If the donor ion signal I_B^∞ is more intense than the acceptor in the pure state, α_A can be greater than unity. The parameter β is proportional to the rate constant, k_{BA}, for the transmission of the charge from a B ion to form an A ion.

Fitting Eqs. (1) or (2) to the intensities for each secondary ion gives values of α and β which relate to that ion as either

donor or acceptor of charge but in which we do not know the precise identity of the partner (ion before or neutral afterwards) fragment involved in any particular exchange. There are very many intense ion fragments for all organic materials so it is likely that more than one charge transfer process actually occurs and is summarized in Eqs. (1) and (2). From α and β, the summary parameter Ξ is determined. Before [7], we have fitted α and β using, for enhancement, $\alpha = [1 - \exp(-\beta)]P + Q\beta$ and, for suppression, $\alpha = \exp(-\beta) - 1$. This removes unwanted correlations in fitting α and β. Thus, for each secondary ion, we fit just β with single values of P and of Q found to be [7] 0.32 and 0.17, respectively. This leads to the same quality of overall fitting as for the separate values of α and β each time. Where this is used, it will be noted. The overall matrix enhancement factor, Ξ, is given by [5].

$$\Xi = \alpha\left(1-(2/\beta) + 2\left\{[1-\exp(-\beta)]/\left(\beta^2\right)\right\}\right) \quad (4)$$

Secondary ions that are enhanced in the mixture have positive Ξ values. The intensity of a secondary ion with a Ξ value of 0, i.e., no enhancement, is linearly correlated with the sample composition. The matrix effect parameters, α, β, and Ξ, are specific to the individual secondary ion and to the identities of the materials A and B. We have measured the α and β values as described by Seah et al. [7].

Results and Discussion

FMOC with Irganox 1010

Firstly, we evaluate the matrix terms for the Irganox 1010/FMOC mixture. We note that the sputtering yield occurs in Eqs. (1) and (2). For 5 keV Ar_{2000}^+ cluster ions, it is not constant for all compositions; it rises for $\phi_{FMOC} > 0.8$, reaching 1.3 times that value at $\phi_{FMOC} = 1$. The yield for 25 keV Bi_3^+ may, or may not, follow a similar trend. In Eqs. (1) and (2), it is not actually the sputtering yield volume that is y but the yield volume from which the secondary ions, rather than the dominating neutrals, are emitted and this may be significantly less [17] than the total sputtered volume and may, or may not, vary with the mixture composition.

So, we may deduce the matrix effect parameters using the intensities generated for each of the two pure materials and three intermediate mixtures, all normalized to the pure Irganox 1010 or FMOC intensities (all use the same 25 keV Bi_3^+ ion dose). If we include the factor y/y_A with $y/y_A = 1.3$ at $\phi_{FMOC} = 1$, the quality of the fitting of Eq. (1) deteriorates from an RMS scatter below 0.01, rising to 0.062. We can see why this occurs by using Eqs. (1) or (2), scaled down by a factor H_i (which could be 1, 1.3, or, say, any value in between to represent the relative sputtering yield) determined by fitting each ion without the $\phi_{FMOC} = 1$ point. With the three data points, H_i is uniquely determined for each secondary ion. Figure 1 shows the fitting for several ions exhibiting a range of Ξ values. For the 56 FMOC secondary ions with signal levels of more than 1000 counts, the factor H_i is found by the fitting to be, on average, 1.005 with a standard deviation of 0.033 and a standard deviation of the mean of 0.004. This differs insignificantly from 1.0 and is not 1.3. In the work that follows, therefore, we assume that the yield volume for the emitted secondary ions does not change with the mixture composition. The data then fit with an average scatter of 0.002, leading to an uncertainty in Ξ of < 0.01.

The matrix factors are measured for 95 secondary ions of Irganox 1010 and 95 of FMOC with minimum intensities of 1500 and 250 counts, respectively, summed over 25 adjacent spectra for that ion in the plateau regions of the profiles for each defined mixture. The lower minimum used for FMOC occurs as the total emitted FMOC intensity is only about 9% of that from Irganox 1010. The matrix factors are shown in Figure 2.

In Figure 2, nearly all the Irganox 1010 matrix factors are negative whereas those for FMOC are nearly all positive. Furthermore, there is a scatter with m/z but the mean result diverges from zero as m/z increases in both cases. If all the fragments have similar kinetic energies, then the time available for the charge transfer to occur will depend on $(m/z)^{0.5}$ and, since β is related to the product of the relevant rate constant and the total interaction time, then β, and hence Ξ, both increase with $(m/z)^{0.5}$. This correlation is shown in Figure 3 for $m/z <$ 250 where, for illustration purposes, the Irganox 1010 data have been plotted with negative $(m/z)^{0.5}$ values.

Figure 3 shows that, up to $m/z = 250$, there is a broad dependence of the matrix factors on $(m/z)^{0.5}$. In Figure 2, it is clear that, for close masses, the details of the fragment structure are also very important. We next look at how the fragment details affect the matrix factor values but first we need to look at the Irganox 1010 and FMOC structures themselves, as shown in Figure SM 1 in the Supplemental Materials. The fragments with added or subtracted hydrogen atoms are easiest to classify and so we study several relatively intense ion sequences from Irganox 1010.

We shall consider the fragments measured for Irganox 1010 shown in Figure SM 1a with selected groups removed and then a number h of hydrogen atoms added or removed. These are shown in Table 1. In Figure SM 1a, are also shown, in yellow, the groups lost for the fragments identified in Table 1 as B, D, and G. C has three lots of B and a carbon atom, E has the sum of D and B, F has two lots of D, and G has almost a complete side chain removed. Figure 4a shows an expansion at high m/z of Figure 2a for these groups. Added are straight lines representing the fits to the data all with the same gradient of − 0.026 per m/z.

In the case of FMOC, there are far fewer hydrogen atoms and so we concentrate on the fragments associated with the aromatic group at the bottom left of Figure SM 1b with up to 13 carbon and nine hydrogen atoms as described in Table 2 and shown in Figure 4b. Added to that figure are straight lines representing the fits to the data all with the same gradient of 0.24 per m/z.

Figure 4 shows some of the systematic effects that occur in Figure 2. In Figure 4a for Irganox 1010, it is shown that losing a

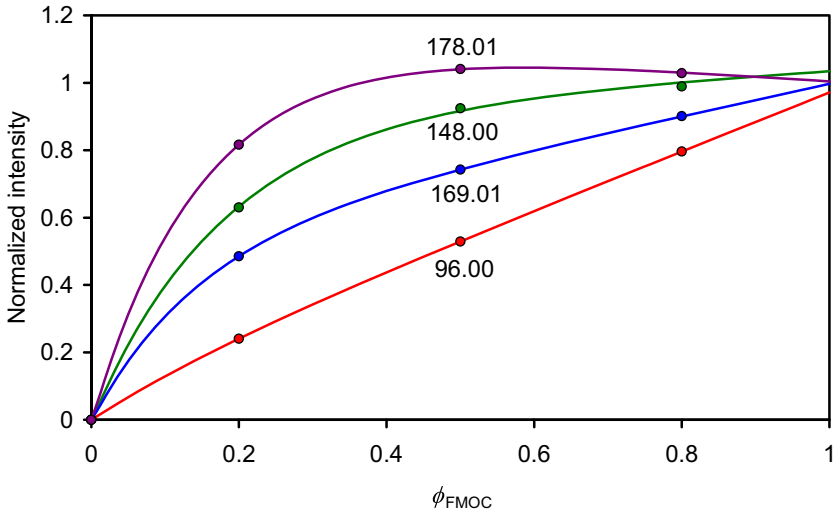

Figure 1. Fitting of the intensity data normalized to that of pure FMOC intensity, as discussed in the text, for $\varphi_{FMOC} = 0, 0.2, 0.5$, and 0.8 with the results of Eqs. (1) and (2) reduced by H_i to determine the values of H_i for each ion for four example negative secondary ions. The pure FMOC ordinate point at (1,1) is not used in the fitting

hydrogen atom makes the matrix factor weaker, i.e., the transference of an electron from the Irganox 1010 to FMOC, or the transference of a proton in the reverse direction, gets more difficult or less probable with each successive hydrogen atom loss. Similarly, in Figure 4b for FMOC, it appears that losing a hydrogen atom again makes the matrix factor weaker, i.e., the

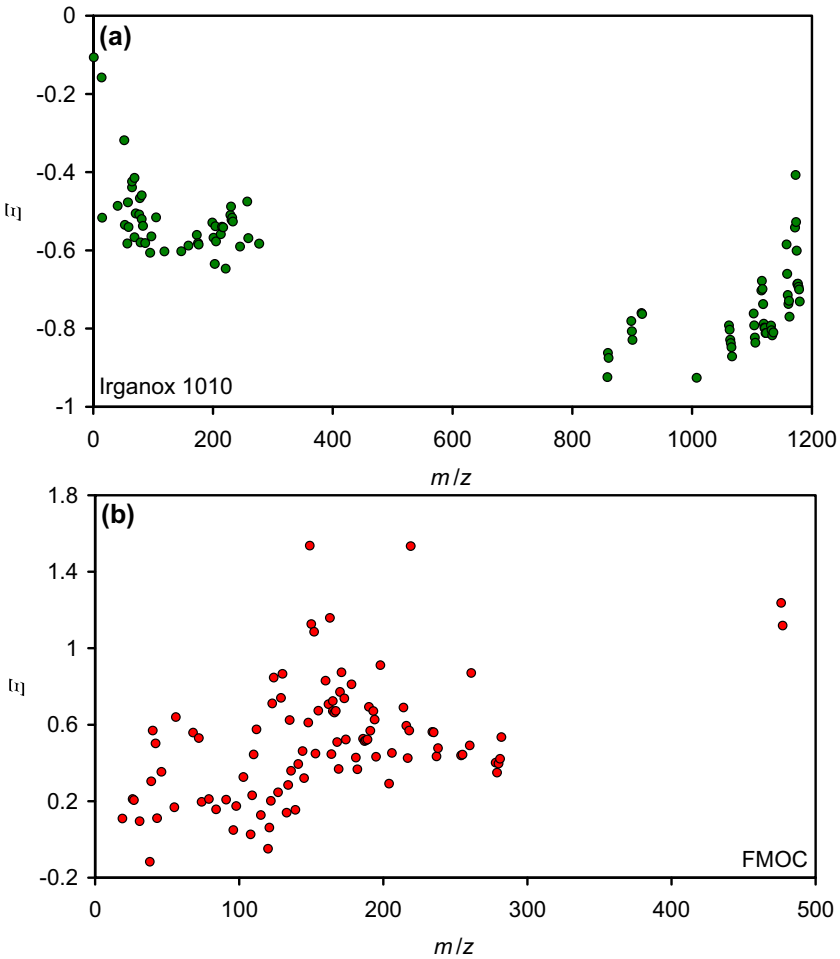

Figure 2. (**a**), (**b**) Measured matrix factors for negative secondary ions from Irganox 1010 and FMOC in Irganox 1010/FMOC mixtures as a function of *m/z*

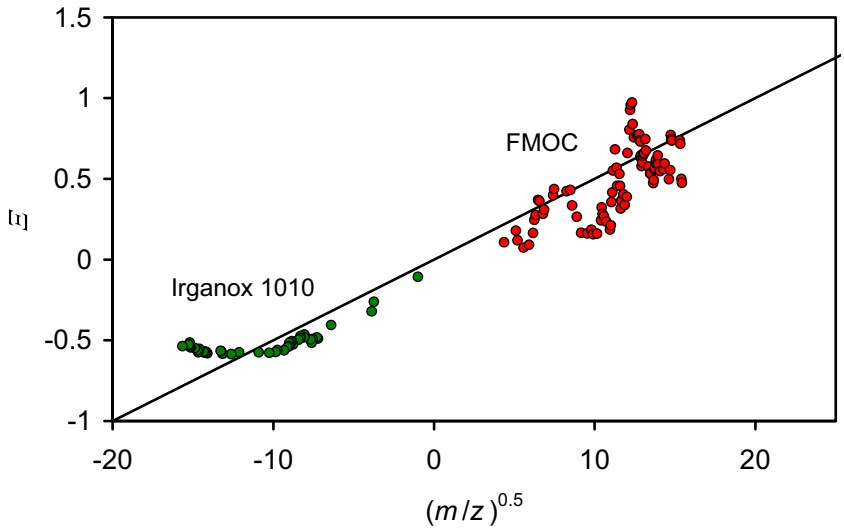

Figure 3. The data from Figure 2 plotted versus $(m/z)^{0.5}$ with the Irganox 1010 plotted with negative m/z values to illustrate the broad $(m/z)^{0.5}$ dependence. The data have been averaged over five adjacent secondary ion masses and are limited to $m/z < 250$

charge transfer gets more difficult or less probable. The gradients of the change in Ξ per hydrogen atom loss are significantly different with the FMOC having nine times greater gradient. This is the same as the ratio of the numbers of H atoms attached to carbon in each of the two molecules.

Analysis using the weaker peaks in Irganox 1010 shows that similar results to those shown in Figure 4a occur in the m/z range up to 300 but with more scatter. The longer sequences that are visible at higher masses in Figure 4a are, unfortunately, not available at low mass, for either material. From these few data, it appears that, in this system, the gradients for addition or removal of an H atom may be similar over a wide mass range.

Figure 4 is clear but the effect in Ξ probably arises from a change in β. The Irganox 1010 data are the most easily investigated. In fitting Eq. (2) to the Irganox 1010 data, these secondary ions all have α values sufficiently close to -1 that they may all be set at -1 and β, which is proportional to the transfer rate constant k, may then be plotted as shown in Figure 5a. In Figure 4a, it is clear that the bottom end of the lines cannot fall below -1 since the minimum value of Ξ is -1. In Figure 5a, there is no such restriction. The extension to negative β values is simply equivalent to switching from suppression to enhancement. It is clear that β increases linearly with the number of hydrogen atoms added or subtracted from each cluster group. We introduce a hydrogen parameter to describe the number of hydrogen atoms in the ion minus a reference number for the master fragment, h, plus the number of broken carbon bonds, b, i.e., it would be the number of hydrogen atoms if those bonds were saturated. Additionally, there will be an offset that clearly depends on the group lost and that may be written many ways. For simplicity, we consider the number of carbon atoms in the ion, N_C, and a fixed offset S such that

$$\beta = m(h + b - pN_C + S) \tag{5}$$

where the parameters m, p, and S are found by fitting. Here, with $m = 0.67$, $p = 0.68$, and $S = 57.4$, the standard deviation in the fit for β is 0.73 which translates to the very small standard deviation of 0.01 in Ξ. Simplifying Eq. (5), by removing b, leads to a degradation of this standard deviation to 0.92. We ignore group G, here, since that also involves oxygen loss and adding an extra parameter for the oxygen would result in a good fit as there is only the one oxygen loss-containing group. The data in Figure 5a are replotted versus $h + b - pN_C + S$ in Figure 5b where each set is separately color coded. This shows more clearly the linearity and consistency of the sets.

Equation (5) may thus be rewritten in a simpler form by rearranging terms:

$$\beta = m(h + b - pc) + \beta_0 \tag{6}$$

where c is the N_C value minus that for the molecular ion (73) and β_0, the value for the molecular ion, is found to be 5.2.

These correlations are very good and show that the fewer the number of hydrogen atoms, the smaller the Ξ values found for ions with usable intensities. However, for the matrix effect to reduce to zero, we need to be well below the masses of the peaks measured and the intensities are then very low. This is unfortunate since identification of the characteristics of ions with zero matrix effect would make quantitative analysis much simpler.

Table 1. Fragments of Irganox 1010 Analyzed with Parameters

Fragment ion group	Main group lost	h range	Carbon bonds broken, b	No. of carbon atoms, N_c	Intensity
A	None	−5 to 3	0	73	Strong
B	CH_3	−3 to 2	1	72	Medium
C	$(CH_3)_3$	3 to 7	3	70	Weak
D	$C(CH_3)_3$	−3 to 5	1	69	Strong
E	$C_4H_9 + CH_3$	0 to 3	2	68	Medium
F	$(C_4H_9)_2$	1 to 6	2	65	Strong
G	R-CH_2	0 to 2	1	56	Medium

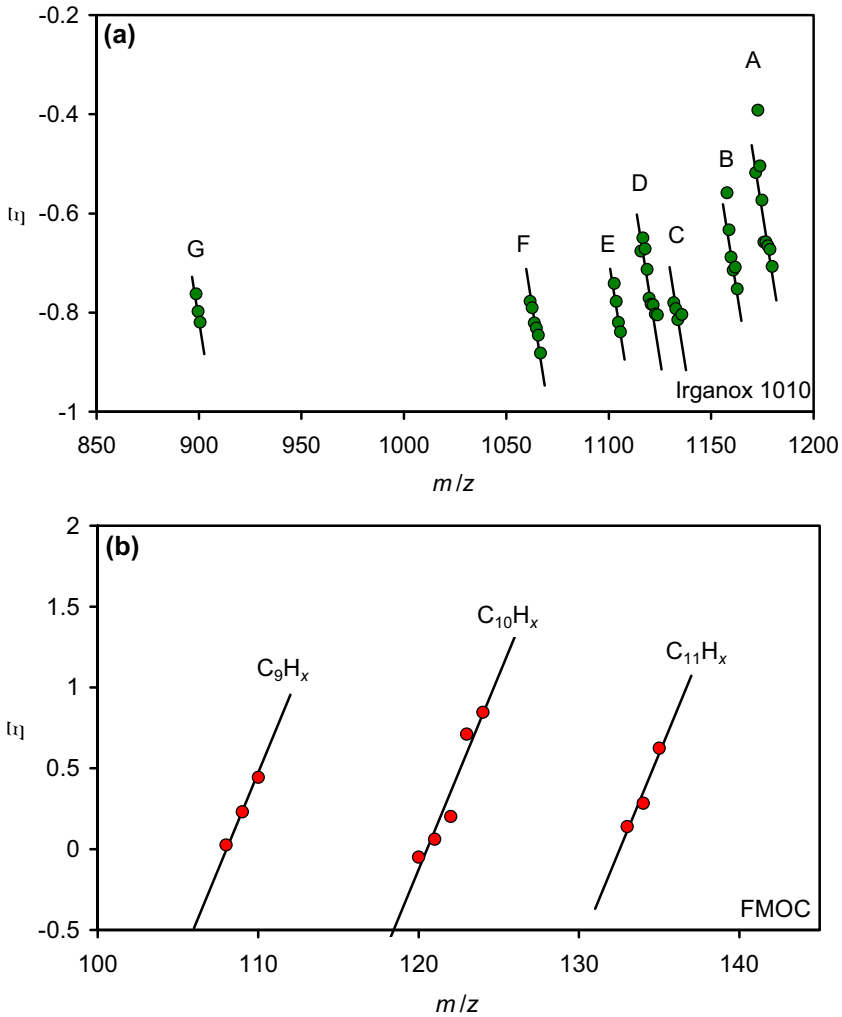

Figure 4. Measured enhancement factors, Ξ, for selected groups of negative secondary ions labeled as in Tables 1 and 2, (**a**) Irganox 1010 (*m/z* 1176.7) and (**b**) FMOC (*m/z* 477.1). The straight lines pass through the centers of mass for each group of data points but have gradients of – 0.026 per *m/z* for Irganox 1010 and 0.24 for FMOC

Note also that the molecular and pseudo molecular ions have significant, but different, matrix effects simply because they have many associated hydrogen atoms.

An equivalent analysis for FMOC is not so easy since the value of α now can be above unity and vary with the fragment. The observed variation in β then depends critically on the value of α and that leads to increased uncertainty in the analysis.

It is interesting to consider the values of β in Figure 5 and see if they are reasonable for likely rate constants. These rate constants are not available for SIMS but are for gas-phase reactions for both electron [24, 25] and proton [26–28] transfer where rate constants of (0.5 to 5) 10^{-15} m^3/s per entity may be found. Shard et al. [4] derive for the enhanced species, "e", that

$$\beta_e = \frac{k t_R \alpha_e Y_e}{V} \quad (7)$$

where k is the rate constant for the charge transfer over a total interaction time t_R in the interaction volume V. α_e is the fraction of the neutral species to be enhanced in the interaction volume and Y_e is the sputtering yield of the neutral fragment being enhanced, when pure, in number emitted per sputtering ion.

We now need to estimate some parameters. The emitted ions and neutrals will have a range of velocities and rough estimates may be taken from the study of Samartsev et al. [29]. There, neutral In atoms sputtered from an indium target by 10 keV Au^-, Au_2^-, and Au_3^- ions have average velocities of 700 m/s that yield an interaction time, t_R, of 14×10^{-13} s. In a molecular dynamics study of the sputtering of polymers by buckminsterfullerene projectiles, Delcorte and Garrison [30] find the average velocity of *m/z* fragments around 1000 Da is

Table 2. Fragments of FMOC Analyzed with Hydrogen Number, *x*

Ion group	*x* range	Intensity
C_9H_x	0 to 2	Strong
$C_{10}H_x$	0 to 4	Medium
$C_{11}H_x$	1 to 3	Weak

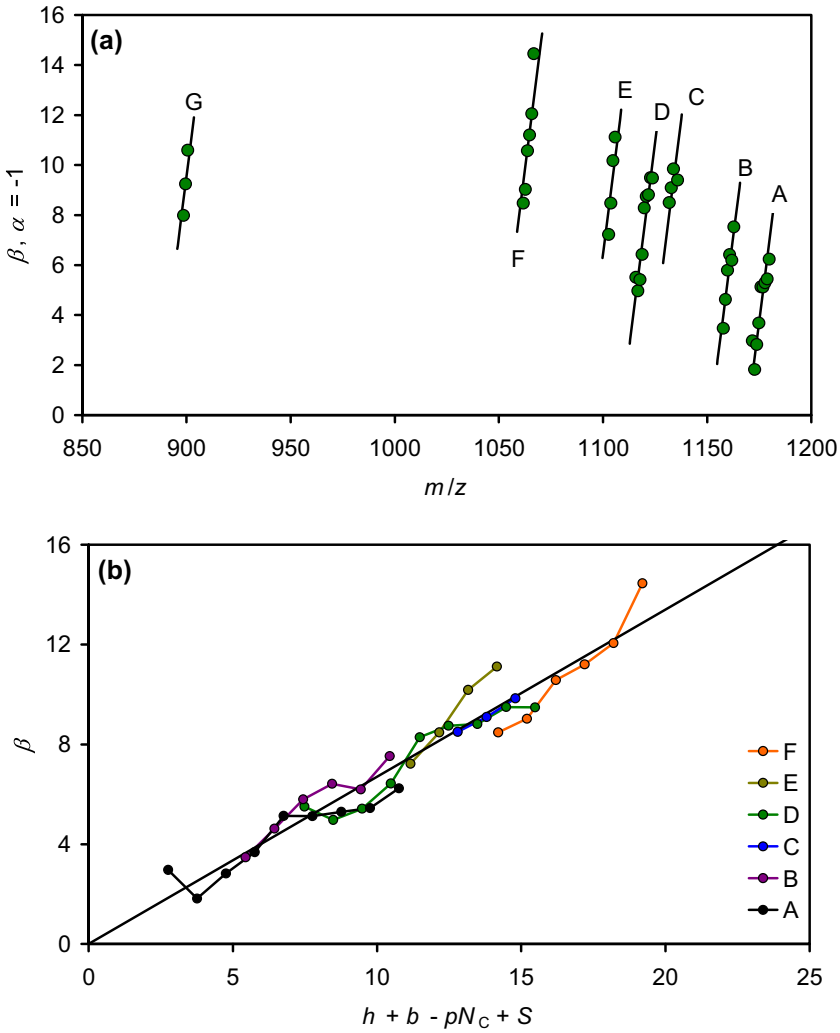

Figure 5. Values of β for sequential groups of negative secondary ions for Irganox 1010 (**a**) fragment ion groups A to G as a function of *m/z*, the straight lines pass through the centers of mass for each group but have the same gradients of 0.67 per *m/z*, and (**b**) groups A to F as a function of the increase in number of hydrogen atoms for each fragment group through $h + b - pN_C + S$

again 700 m/s. Ions appear to have slightly higher median energies [31] than neutrals and hence lower interaction times but this difference is less than a factor of 2 so an estimate for t_R could be 14×10^{-13} s per nm of interaction path. If, for Eq. (7), we take α_e as -1 (the Irganox 1010 fragments show suppression), the fragment yield Y_e as ~ 1 (Y_e here is the number of relevant neutral fragments emitted per incident ion not a yield volume), the interaction volume, V, as similar to the fragment size of 1.5 nm^3, we find β values in the range 0.5 to 5. It appears that the rate constants are similar for electron and proton exchange. Although these calculations are not precise, this estimated range for β is that observed here and elsewhere [23] and supports this general approach.

Irganox 1098 and Irganox 1010

The Irganox 1098 molecule has great similarities with Irganox 1010. It is comprised of two of the four Irganox 1010 side chains from the -(C=O)- group outwards, joined in the middle by -(NH)-$(CH_2)_6$-(NH)-. So, it is about half the mass, size, and molecular weight of the Irganox 1010 molecule but with a similar relative hydrogen content. Such similarity means that strong matrix effects between these two molecules are not expected. The total negative ion yield of the Irganox 1098 is 1.08 times that for Irganox 1010. Figure 6a shows the measured matrix factors for many ion characteristic of both materials. The matrix factors are about one third of those for FMOC/Irganox 1010 mixtures and generally show a smaller ion-to-ion scatter. The uncertainties here are estimated to be 0.05. Most ions show values of Ξ around zero, as expected from the similarities of the two molecular structures. Close to the molecular ion, the Irganox 1098 ions have increased matrix values, whereas those for Irganox 1010 show the reverse effect. This is shown more clearly in Figure 6b where the abscissa plots the change in the *m/z* value from that for the molecular ion in each case. The general trends appear complementary in that the Irganox 1010 ions have increasingly negative matrix factors to a similar extent that the Irganox 1098 become positive. The red and green dotted

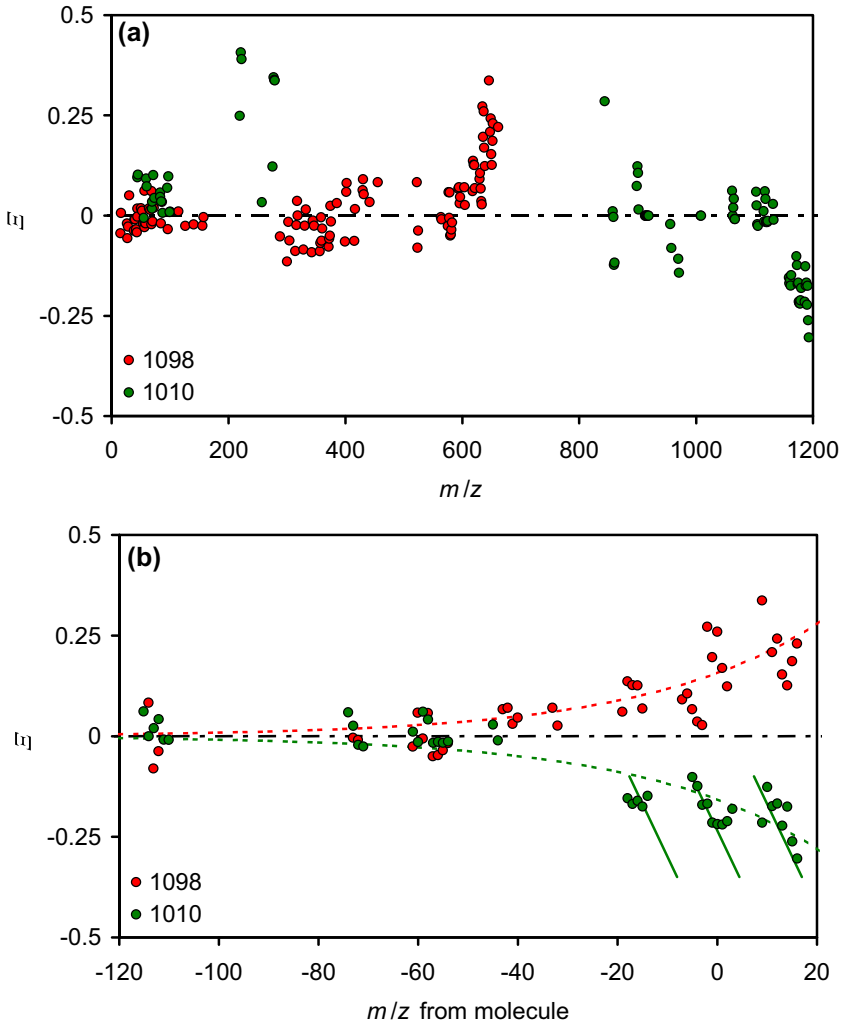

Figure 6. Measured matrix factors for negative secondary ions from Irganox 1098 and Irganox 1010 in their mixtures, (**a**) as a function of *m/z* and (**b**) as a function of the change in the *m/z* value from that for the molecular ion. In (**b**), the dotted curves are symmetrical curves showing the general trends and the solid green lines show the gradients of – 0.026 per hydrogen atom from Figure 4a

curves show this symmetry. For adjacent ions, the effects are not complementary but are similar. They both show increasing values of matrix factor for each hydrogen loss, superimposed on the general trends shown by the dotted lines. The solid green lines for adjacent mass ions have a gradient of − 0.026 per hydrogen atom as shown in Figure 4a which is the value also found for Irganox 1010 when with FMOC. So while the Irganox 1010 pseudo molecular ions generally transfer charge to those of Irganox 1098, each hydrogen loss for both molecules sees the fragments, more and more, retain their charge or gain it from others, i.e., for both materials the matrix factors tend towards more positive values for each hydrogen loss.

Ir(ppy)2(acac) and Irganox 1010

The Ir(ppy)2(acac) molecule, shown in Figure SM 2, generates 2.1 times the total negative ion yield of that of Irganox 1010. Sequences of ions with one hydrogen loss could involve the groups on the right of the diagram.

Figure 7 shows the measured Ξ values for both positive and negative ions for both materials. Many peaks from Irganox 1010 seen in the previous plots are not available here since for ions at those mass values there are, unfortunately, contributions from both materials. As before, the Irganox 1010 appears to be promoting the ion yield of the other material and exhibits negative Ξ values. The ranges of data are similar to those for Irganox 1010 with FMOC. As with FMOC, the Ir(ppy)2(acac) Ξ values rise with *m/z* (with some scatter) but then at *m/z* in the 150 to 300 range, start to fall again. The FMOC data were unclear in that region. Note that for $m/z > 600$, one must be dealing with more than one Ir(ppy)2(acac) molecule or parts of molecules which will not necessarily behave as described by Eqs. (1) and (2) and so those data are shown by a solid line which follows the track of the median values. The

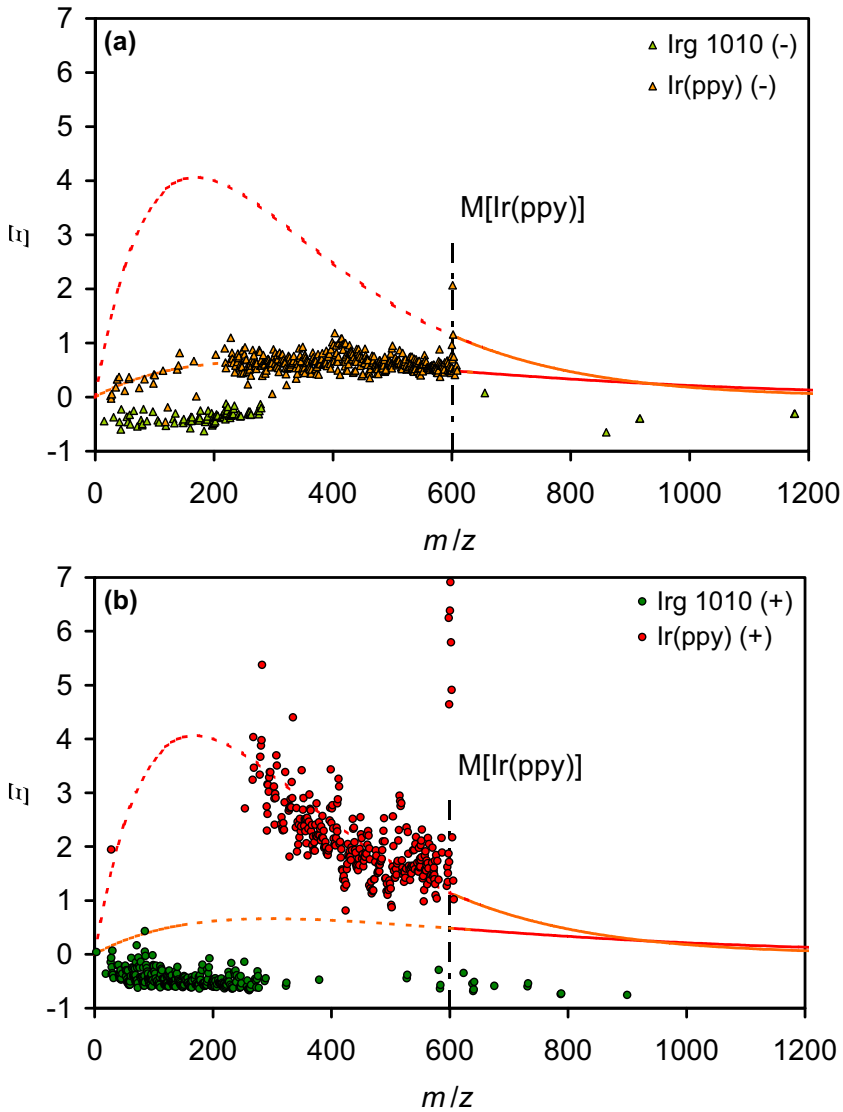

Figure 7. Measured matrix factors (**a**) for negative (–) and (**b**) positive (+) secondary ions of Ir(ppy)2(acac) and Irganox 1010 in their mixtures, as a function of *m/z*. The red and orange curves pass through the centers of the Ir(ppy) ion distributions and are to guide the eye. They have the simple form $(m/z)\exp[-(m/z)/(m_0/z)]$ and are dashed for masses below, and solid above, the Ir(ppy) molar mass

enhancement for the emitted positive secondary ions is very much stronger than for negative ions.

The Ir(ppy)2(acac) data in Figure 7 do not show the clear sequences of data shown in Figure 4 and that may be due to the same mass fragment arising from losses at both the left and the right hand ends of the molecule involving very different components.

In Figure 7, for masses below $m/z = 600$, the solid lines for both positive and negative secondary ions continue as dashed lines approximately describing the data. At the higher masses, these more intact fragments arise from the outer, cooler, part of the impact crater where the interaction geometry for charge transfer gets less and less favorable and hence Ξ falls as m/z increases—the charged and uncharged entities generally having a weaker interaction when coming from different regions of the impact crater. This general result for the enhanced species, with a maximum in the $m/z = 150$ to 300 range, would be good to test in many other systems. In the low-mass region, the highly fragmented secondary ions are thought to arise from the more energetic central zone of the impact crater.

This general result does not of course describe the changes between successive ions in the spectrum and of particular interest to analysts is the behavior for secondary ions close to the molecular ion. Figure 8 shows how Ξ changes as a hydrogen atom is added to (shown by the arrow direction) or removed from the molecular secondary ion (represented by the larger symbol in each case). For the negative secondary ions, the $(M-H)^-$ ion is the most intense with the $(M)^-$ ion having 30 to 70% of its intensity. In each case, Ξ changes as the number of hydrogen atoms increases. For the positive secondary ions, which have the stronger matrix terms, the $(M)^+$ ion is the most intense and the changes in Ξ are much greater. We do not know if this is general since few other such measurements of both positive and negative secondary ions are reported.

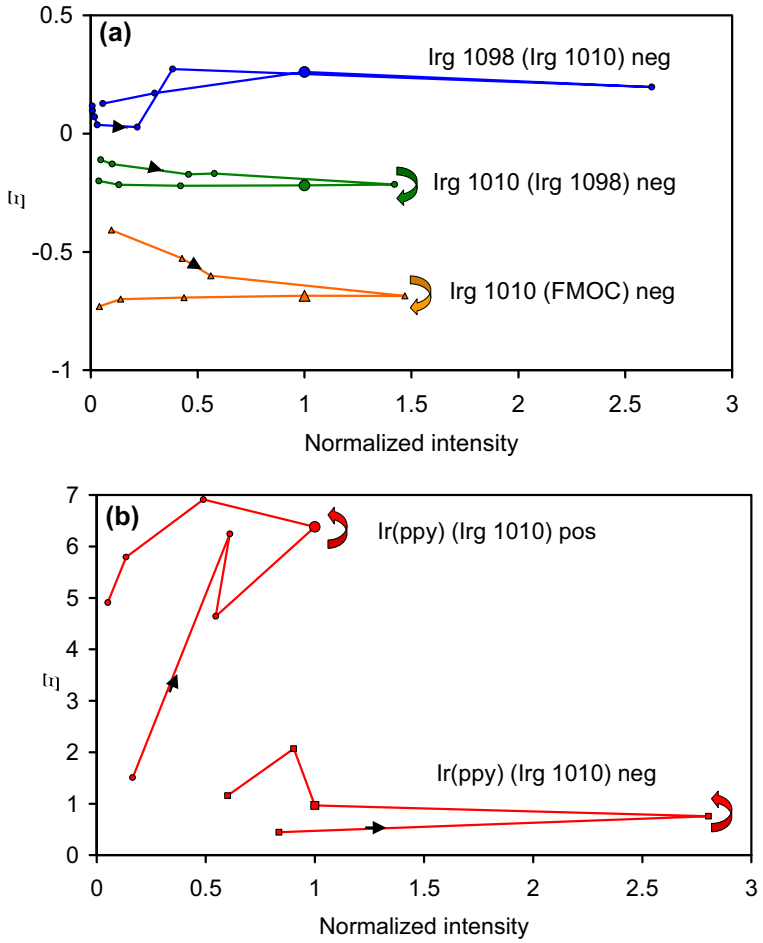

Figure 8. The variations in Ξ as a function of the intensity normalized to that of the molecular group, for each material for pseudo molecular ions of the material indicated (mixture material in brackets). The arrows show the direction of adding hydrogen atoms. In (**a**), the orange line with triangles is for negative secondary ions of Irganox 1010 from the Irganox 1010/FMOC sample; the dark green and blue with circles are for negative secondary ions of Irganox 1010 and Irganox 1098, respectively, from that pair of materials. In (**b**), the red lines with squares and circles are for negative and positive secondary ions, respectively, of Ir(ppy)2(acac) from the Irganox 1010/Ir(ppy)2(acac) sample

Conclusions

Matrix effects have been measured in detail for the negative secondary ions for three organic mixtures involving Irganox 1010 and for positive secondary ions for one mixture. In all cases, transference of charge is seen from Irganox 1010 to the other material. In the mixture with FMOC, the matrix factors for Irganox 1010 fall as low as − 0.9 whereas those for FMOC rise to nearly 2. For $m/z < 250$, the matrix factors scale very roughly with $(m/z)^{0.5}$, supporting an effect that depends on the interaction time and hence the ion velocity. Low-mass ions have in general lower matrix factors but values may reach as high as 0.5 by $m/z = 50$. Analysis of groups of ions with addition or loss of a hydrogen atom shows that the matrix factors of the Irganox 1010 and FMOC ions change by approximately − 0.026 and 0.24 per hydrogen atom, respectively. The relative changes may be associated with the numbers of hydrogen atoms available for the charge transfer, there being many more available in Irganox 1010 than FMOC. For Irganox 1010, it is shown that the change arises from the change in the transference rate constant as the number of hydrogen atoms increases and the number of carbon atoms reduces. Data for the Irganox 1098 and Irganox 1010 system show much weaker matrix effects since the two molecules have significant chemical similarities. Matrix factors reach 0.3 and − 0.3 for the pseudo molecular ions from Irganox 1098 and Irganox 1010, respectively. For these ions, both show matrix factors that change by approximately − 0.026 per hydrogen atom increase. For the third system of Irganox 1010 with Ir(ppy)2(acac), the transference of both positive and negative charge is again from the Irganox 1010. The matrix terms for the negative secondary ions are again strong but those for the positive ions are much stronger. Here, it is clear that the matrix terms do not increase beyond $m/z = 300$ but slowly decline. This is attributed to a geometrical effect associated with the central part of the Bi_3^+ impact crater from which the more energetic fragmented ions of low mass arise compared with the rim of the crater from which the pseudo molecular ions of high mass are emitted. All

data are precisely described by Shard et al.'s [5] charge transfer model. We see, overall, effects of ion velocity, fragment chemistry, and the point of origin of the secondary ion to be significant. Analysis of the molecular and pseudo molecular ions shows significant matrix effects that change from fragment to fragment showing that these ions, too, cannot be used directly for quantitative analysis.

Acknowledgements

The authors would like to thank M. Wywijas and S. A. Smith for the preparation of the samples used in this study and A G Shard for helpful comments. This work forms part of the "3D OrbiSIMS" project in the Life-science and Health programme of the National Measurement System of the UK Department of Business, Energy and Industrial strategy. This work has received funding from the 3DMetChemIT project of the EMPIR programme co-financed by the Participating States and from the European Union's Horizon 2020 research and innovation programme.

Compliance with Ethical Standards

Conflict of Interest The authors declare that they have no competing interests.

References

1. Jones, E.A., Lockyer, N.P., Vickerman, J.C.: Suppression and enhancement of non-native molecules within biological systems. Appl. Surf. Sci. **252**, 6727–6730 (2006)
2. Karras, G., Lockyer, N.P.: Quantitative surface analysis of a binary drug mixture – suppression effects in the detection of sputtered ions and post-ionized neutrals. J. Am. Soc. Mass Spectrom. **25**, 832–840 (2014)
3. Alnajeebi, A.M., Vickerman, J.C., Lockyer, N.P.: Matrix effects in biological SIMS using cluster ion beams of different composition. BioInterphases. **11**, 02A317-1–02A317-4 (2016)
4. Shard, A.G., Rafati, A., Ogaki, R., Lee, J.L.S., Hutton, S., Mishra, G., Davies, M., Alexander, M.R.: Organic depth profiling of a binary system: the compositional effect on secondary ion yield and a model for charge transfer during secondary ion emission. J. Phys. Chem. B. **113**, 11574–11582 (2009)
5. Shard, A.G., Spencer, S.J., Smith, S.A., Havelund, R., Gilmore, I.S.: The matrix effect in organic secondary ion mass spectrometry. Int. J. Mass Spectrom. **377**, 599–609 (2015)
6. Seah, M.P., Shard, A.G.: The matrix effect in secondary ion mass spectrometry. Appl. Surf. Sci. **439**, 605–611 (2018)
7. Seah, M.P., Havelund, R., Gilmore, I.S.: SIMS of delta layers in organic materials – amount of substance, secondary ion species, matrix effects and anomalous structures in argon gas cluster depth profiles. J. Phys. Chem. C. **120**, 26328–26335 (2016)
8. Havelund, R., Seah, M.P., Gilmore, I.S.: SIMS of organic materials – interface location in argon gas cluster depth profiles. J. Am. Soc. Mass Spectrom. **29**, 774–785 (2018)
9. Delcorte, A.: Matrix-enhanced secondary ion mass spectrometry: the Alchemist's solution. Appl. Surf. Sci. **252**, 6582–6587 (2006)
10. Jones, E.A., Lockyer, N.P., Kordys, J., Vickerman, J.C.: Suppression and enhancement of secondary ion formation due to the chemical environment in static-secondary ion mass spectrometry. J. Am. Soc. Mass Spectrom. **18**, 1559–1567 (2007)
11. Mouhib, T., Delcorte, A., Poleunis, C., Bertrand, P.: Organic secondary ion mass spectrometry: signal enhancement by water vapor injection. J. Am. Soc. Mass Spectrom. **21**, 2005–2010 (2010)
12. Sheraz, S.n.R., Barber, A., Fletcher, J.S., Lockyer, N.P., Vickerman, J.C.: Enhancing secondary ion yields in time of flight-secondary ion mass spectrometry using water cluster primary beams. Anal. Chem. **85**, 5654–5658 (2013)
13. Sheraz, S.n.R., Razo, I.B., Kohn, T., Lockyer, N.P., Vickerman, J.C.: Enhancing ion yields in time-of-flight-secondary ion mass spectrometry: a comparative study of argon and water cluster ion beams. Anal. Chem. **87**, 2367–2374 (2015)
14. Angerer, T.B., Pour, M.D., Malmberg, P., Fletcher, J.S.: Improved molecular imaging in rodent brain with time-of-flight-secondary ion mass spectrometry using gas cluster ion beams and reactive vapor exposure. Anal. Chem. **87**, 4305–4313 (2015)
15. Tian, H., Wucher, A., Winograd, N.: Reduce the matrix effect in biological tissue imaging using dynamic reactive ionization and gas cluster ion beams. Biointerphases. **11**, 02A3210-1–02A3210-5 (2016)
16. Shard, A.G., Havelund, R., Spencer, S.J., Gilmore, I.S., Alexander, M.R., Angerer, T.B., Aoyagi, S., Barnes, J.-P., Benayad, A., Bernasik, A., Ceccone, G., Counsell, J.D.P., Deeks, C., Fletcher, J.S., Graham, D.J., Heuser, C., Lee, T.G., Marie, C., Marzec, M.M., Mishra, G., Rading, D., Renault, O., Scurr, D.J., Shon, H.K., Spampinato, V., Tian, H., Wang, F.Y., Winograd, N., Wu, K., Wucher, A., Zhou, Y.F., Zhu, Z.H.: Measuring compositions in organic depth profiling: results from a VAMAS interlaboratory study. J. Phys. Chem. B. **119**, 10784–10797 (2015)
17. Havelund, R., Seah, M.P., Gilmore, I.S.: Sampling depths, depth shifts and depth resolutions for bi_n^+ ion analysis in argon gas cluster depth profiles. J. Phys. Chem. B. **120**, 2604–2611 (2016)
18. Seah, M.P., Gilmore, I.S., Spencer, S.J.: Quantitative XPS I: analysis of X-ray photoelectron intensities from elemental data in a digital photoelectron database. J. Electron Spectrosc. Relat. Phenom. **120**, 93–111 (2001)
19. Tables of average matrix sensitivity factors are available at http://www.npl.co.uk/science-technology/surface-and-nanoanalysis/services/xps-and-aes-average-matrix-relative-sensitivity-factors
20. ISO 18118:2015 – Surface chemical analysis Auger electron spectroscopy and X-ray photoelectron spectroscopy – guide to the use of experimentally determined sensitivity factors for the quantitative analysis of homogeneous materials. ISO Geneva (2015)
21. Seah, M.P.: A system for the intensity calibration of electron spectrometers. J. Electron Spectrosc. Relat. Phenom. **71**, 191–204 (1995)
22. Transmission function correction software is available at http://www.npl.co.uk/science-technology/surface-and-nanoanalysis/services/calibration-software-and-reference-materials-for-electron-spectrometers
23. Seah, M.P., Havelund, R., Shard, A.G., Gilmore, I.S.: Sputtering yields for mixtures of organic materials using argon gas cluster ions. J. Phys. Chem. B. **119**(13), 433–13,439 (2015)
24. Eichelberger, B.R., Snow, T.P., Bierbaum, V.M.: Collision rate constants for polarizable ions. J. Am. Soc. Mass Spectrom. **14**, 501–505 (2003)
25. Nichols, C.M.: Gas-phase ion chemistry: kinetics and thermodynamics. Ph D Thesis, University of Central Arkansas (2009)
26. Su, T., Bowers, M.T.: Ion-polar molecule collisions: the effect of ion size on ion-polar molecule rate constants, the parameterization of the average-dipole-orientation theory. Int. J. Mass Spectrom. **12**, 347–356 (1973)
27. Celli, F., Weddle, G., Ridge, D.P.: On statistical and thermodynamic approaches to ion-polar molecule collisions. J. Chem. Phys. **73**, 801–812 (1980)
28. Zhao, J., Zhang, R.: Proton transfer reaction rate constants between hydronium ion (H_3O^+) and volatile organic compounds. Atmos. Environ. **38**, 2177–2185 (2004)
29. Samartsev, A.V., Duvenbeck, A., Wucher, A.: Sputtering of indium using Au_m projectiles: transition from linear cascade to spike regime. Phys. Rev. B. **72**, 115,417 (10 pages (2005)
30. Delcorte, A., Garrison, B.J.: Sputtering polymers with buckminsterfullerene projectiles: a coarse-grain molecular dynamics study. J. Phys. Chem. C. **111**(15), 312–15,324 (2007)
31. Mazarov, P., Samartsev, A.V., Wucher, A.: Determination of energy dependent ionization probabilities of sputtered particles. Appl. Surf. Sci. **252**, 6452–6455 (2006)